*J. Synchrotron Rad.* (1995). **2**, 119–123

# Adaptive Silicon Monochromators for High-Power Wigglers; Design, Finite-Element Analysis and Laboratory Tests

**J. P. Quintana[a] and M. Hart[b]**

*[a]DND-CAT Synchrotron Research Center, APS/ANL Sector 5, Building 400, 9700 South Cass Avenue, Argonne, IL 60439, USA, and [b]Department of Physics, Schuster Laboratory, The University, Manchester M13 9PL, UK*

*(Received 6 March 1995; accepted 22 March 1995)*

Multipole wigglers in storage rings already produce X-ray power in the range up to a few kilowatts and planned devices at third-generation facilities promise up to 30 kW. Although the power density at the monochromator position is an order of magnitude lower than that from undulators, the thermal strain field in the beam footprint can still cause severe loss of performance in X-ray optical systems. For an optimized adaptive design, the results of finite-element analysis are compared with double-crystal rocking curves obtained with a laboratory X-ray source and, in a second paper [Quintana, Hart, Bilderback, Henderson, Richter, Setterson, White, Hausermann, Krumrey & Schulte-Schrepping (1995). *J. Synchotron Rad.* **2**, 1–5], successful tests at wiggler sources at CHESS and ESRF and in an undulator source at HASYLAB are reported.

**Keywords: X-ray optics; high-heat-load optics; adaptive optics; finite-element analysis; wigglers.**

## 1. Introduction

During the last few years, there has been a great deal of experimental and theoretical progress in understanding and solving the problems which confront designers of high-heat-load X-ray optics for synchrotron radiation sources. Much progress has been made and mature designs implemented which remove the heat. Much less attention has been given to the fundamental problem of how to control and (hopefully) to eliminate the thermally induced strain field which corrupts the diffraction profile from the monochromator crystal. The figure of merit relating temperature change to elastic strain is $k/\alpha$ where $k$ is the thermal conductivity and $\alpha$ is the thermal expansivity and both parameters are isotropic. In principle, the mechanical response of a cubic crystal to an inhomogeneous heat load within the thermal footprint is very complicated since the mechanical elastic response is dependent on the mechanical boundary conditions as well as the usually anisotropic material crystal elastic constants. Even the ubiquitous silicon is quite anisotropic and its Young's modulus is 44% larger in ⟨111⟩ directions than in ⟨100⟩ directions (Wortman & Evans, 1965).

Since $k$ becomes very large and $\alpha$ very small at low temperatures, the room temperature ratio of $k/\alpha$ is maximum in materials with a very high Debye temperature. Therefore, diamond and cryogenically cooled silicon-crystal monochromators have been constructed and tested on high-power-density synchrotron beams (Berman, Hastings *et al.*, 1993; Berman & Hart, 1993; Bilderback, 1986; Marot *et al.*, 1992; Sharma, Berman, Hastings & Hart, 1992; Zhang, 1993) at power densities in the 100 W mm$^{-2}$ range. Although these two methods provide solutions to the problems of undulator beam optics, neither at present are suitable for the much larger and higher total power of wiggler beams. Available diamonds are simply too small while present designs for silicon using liquid-nitrogen cooling fail through the onset of boiling at the critical heat flux, above a few hundred watts in current designs (Zhang, 1993).

The alternative is to provide a means by which the crystal monochromator can adapt so as to cancel the thermally induced strain field within the beam footprint (Berman & Hart, 1991*a*,*b*; Berman, Hart & Sharma, 1992; Berman & Hastings, 1992; Hart, 1990; Smithers, 1989). In principle, two separate corrections are required, one which compensates for the cooling gradient normal to the crystal surface and another to provide control of the surface temperature gradient which is present when the effective beam footprint is finite or non-uniform. In earlier experiments (Berman & Hart, 1991*b*) the crystal design was similar to that presented here and the necessary adaptive force was provided by a pneumatic bellows system. In this paper, we have optimized the basic crystal design by finite-element analysis (*ANSYS*; Swanson Analysis Systems Inc., 1994) for the case when the adaptive forces are provided by the coolant pressure itself. Consequently, this design provides the adaption without in-vacuum actuators or transducers. Tests of double-crystal rocking curves *versus* pressure using a laboratory X-ray source confirm the modeling results and tests using the A2 wiggler at CHESS, the W2 wiggler at ESRF and the BW1 undulator at HASYLAB have been reported previously (Quintana, Hart *et al.*, 1995).

## 2. Crystal design

A cut-away view of the crystal assembly is shown in Fig. 1 (Berman & Hart, 1991*a*; Hart, 1990). The ribbon beam of X-rays from the wiggler source impinges symmetrically on the top surface of the silicon-crystal box. It is a line source of power, parallel to the $y$ axis, with a Gaussian heat profile parallel to the $x$ axis. The mounting block and water-jet assembly is made of stainless steel.

There are two principal components in the thermal gradient field so far as the present discussion is concerned. The cooling gradient, $\Delta T_z$, results in a strain field whose lowest order component is a cylindrical bend about the $y$ axis. The surface temperature gradient, $\Delta T_x$, causes the 'thermal bump' and results in a variation of lattice parameter and Bragg angle in the $x$ direction. In earlier experiments, stainless-steel baffles were used to frustrate the jet cooling near the edges of the beam so as to render the top surface of the crystal isothermal, *i.e.* to ensure $\Delta T_x \simeq 0$. In the present experiments, this refinement was not included in either the crystals or the finite-element modeling. The purpose of the experiments was to evaluate the feasibility of active thermal strain-field compensation by controlling the water coolant pressure, *not* to determine a final design with correction for both components of the thermal strain field.

Even in a simple cross section such as that considered here, there are many degrees of freedom in choosing crystal dimensions and boundary conditions. It must be emphasized that finite beam power footprints, such as those which we are forced to accept from wigglers and undulators, produce very complicated strain fields and Bragg-angle variations.

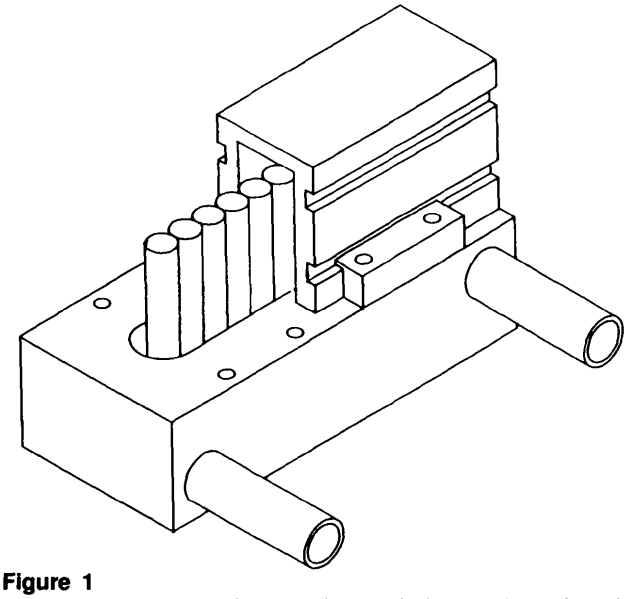

**Figure 1**
Scale diagram of the jet-cooled crystal described herein. The crystal is shown cut away exposing the steel cylindrical cooling jets that protrude from the base. The top surface of the crystal is the (111) diffracting surface and is taken as the $xz$ plane with $z$ parallel to the long dimension of the crystal. The crystal height is parallel to the $y$ axis. Each wall of the crystal contains two built-in 'hinges' that run the entire length of the crystal. The bottom of the lower hinge is held with a safety clamp to the steel base.

For example, $\Delta T_z$ causes an antisymmetric variation of the Bragg angle *versus* $x$, while $\Delta T_x$ produces a symmetric variation. Consequently, in principle, a minimum of two different corrections are required just to compensate the strain-field profile to first order (Berman & Hart, 1991*b*). In reality, the deformation field is more complex when the power profile and penetration depth are taken into account.

## 3. Finite-element analysis

Fig. 2 shows the calculated response of two different crystal cross sections to internal pressure changes; the top surfaces are 1.0 and 2.5 mm thick (Figs. 2*a* and 2*b*, respectively). The overall box cross section is 21 × 28 mm with 5 mm thick walls. It is clear that the shape of the top surface of the silicon box is sensitive to the crystal thickness, and, as we will show later, the aspect ratio (*i.e.* the height-to-width ratio of the silicon box) is the next most important design parameter. The primary objective is to make the diffracting surface concave so as to compensate the convex form generated by the thermal footprint of the wiggler beam.

Important features of the box cross section, which calculations show to be non-critical in dimension, involve several different considerations. The finite-element analysis assumes that $F$, the fixing line in Fig. 2, is a clamped boundary. The two pairs of elastic hinges are 2.5 × 2.0 mm in cross section with the longer dimension parallel to the base. The bottom edge of the lower hinge is located 6 mm from the mounting base. The bottom edge of the upper hinge is set to be equidistant between the bottom edge of the lower hinge and the midplane of the lamella. The exact hinge thickness is not an important parameter since the bending stiffness of the lamella varies with the cube of the thickness and the hinges are at least ten times more compliant than the box walls. In addition to its obvious function, the lower hinge effectively ensures that the mounting strains inherent in joining silicon to stainless steel with silicone rubber do not influence the strain field in the upper part of the silicon box. In this design, this crucial mounting region containing disparate materials is maintained at constant temperature by the flowing coolant. Transfer of the bending moment generated

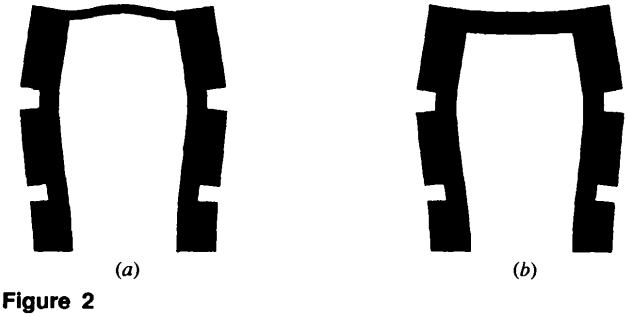


**Figure 2**
Cross-sectional deformation modes under the forces due to coolant pressure inside the silicon box structure. The fixing line $F$ is taken as the horizontal line at the bottom base of the silicon box. (*a*) $t = 1$ mm, (*b*) $t = 2.5$ mm.

by the coolant pressure on the side walls to the top surface requires adequate angular rigidity in the top corners of the silicon box. We expect that the top lamella will deform into a concave cylinder when equal couples are applied to its edges induced by the internal coolant pressure. However, the coolant pressure also acts to push out the top lamella, adding a component to the distortion which is convex. In the current design, the crystal is attached to the base using silicone rubber. Consequently, while the 'clamped boundary' condition is not fully realized, it is still instructive to consider this problem to study the effect of coolant pressure on the lamella shape. In addition, this condition is also relevant for future designs which would rely on a less compliant seal (*e.g.* indium).

### 3.1. *Influence of crystal thickness*

Fig. 3 shows in quantitative detail the inclination of the crystal surface ('slope') *versus* position for the case when the coolant pressure is 100 kPa. Cylindrical bending would be indicated by a linear variation of slope with distance across the crystal in the $x$ direction. We see immediately in Fig. 3 that the thickness of the top face of the silicon box is a critical parameter. It is also interesting to note that the slope at the box edges is not the same in the two cases; the simple model in which the side walls generate a couple along the edges of the top wafer is not perfect because the top wafer is not totally compliant. Whilst the ratio of the bending stiffness for these two cases is $(2.5/1.0\,\text{mm})^3 = 15.6$, the ratio of the slopes is only 1.4. This indicates the qualitative value of the simple model. Over the full width of the 2.5 mm thick silicon box, the shape is within 5.5 μrad of a perfect cylinder. If, for the 2.5 mm top wafer thickness, the width of the silicon box increases, then it is clear that eventually, the center must become concave under the direct influence of the coolant pressure. Thus, the aspect ratio is the second most important design parameter to explore.

In the simple case of a uniform heat input, one-dimensional heat flow results in a uniform curvature $R^{-1} = \alpha(T_h - T_c)/t$ where $t$ is the crystal thickness and $T_h$, $T_c$ are the temperatures at the hot and cold surfaces. Alternatively, $R^{-1} = P\alpha/k$ where $P$ is the power input per unit area at the hot surface. Thus, $P = 1\,\text{W mm}^2$ on silicon causes a curvature of $69\,\text{m}^{-1}$ regardless of crystal thickness or crystallographic orientation. If the width of the Gaussian wiggler footprint is large compared with the crystal thickness, as is usually the case, then heat flow in the central region would be approximately one-dimensional and a cylindrical bend would be expected. This is confirmed by finite-element-analysis modeling (Chrzas, Khounsary, Mills & Vicarro, 1990). With the dimensions shown in Figs. 1 and 2, we see that the 2.5 mm thick crystal is bent concave upward by the coolant pressure into a cylinder and this is just the deformation required to compensate for the thermally induced convex cylinder. The mean curvature for 100 kPa of applied pressure is $-22\,\text{m}^{-1}$. Since the pressure deformation is well within the elastic range, linear extrapolation applies so that 100 kPa water pressure compensates the thermal curvature produced by a footprint power density of $3\,\text{W mm}^{-2}$.

The deformations shown in Figs. 2 and 3 remain similar throughout the range $0 < t \leq 10$ mm; for $t \leq t_0$, the center is always concave upwards while for large $t$ values the entire surface is always concave downwards. At the 'neutral' thickness $t_0$, when the mean curvature is zero, independently of coolant pressure, the crystal surface is not flat but has the same qualitative shape as the thin crystal case (Fig. 2*a*).

### 3.2. *Influence of aspect ratio*

To explore and illustrate the influence of the aspect ratio on the silicon box pressure response we have modeled the deformation for three different box widths, $w$. For the case $w = 21$ mm, the deformable central lamella is 12 mm wide. We also considered lamella 20 and 28 mm wide corresponding to $w = 29$ and 37 mm, respectively. Figs. 4 and 5 show the results of finite-element-analysis modeling for the two characteristic thicknesses $t = 1$ and 2.5 mm evaluated at 100 kPa water pressure. The central region of the thin crystal (Fig. 4) always becomes convex upwards, that is, the gradient of the slope *versus* $x$ position

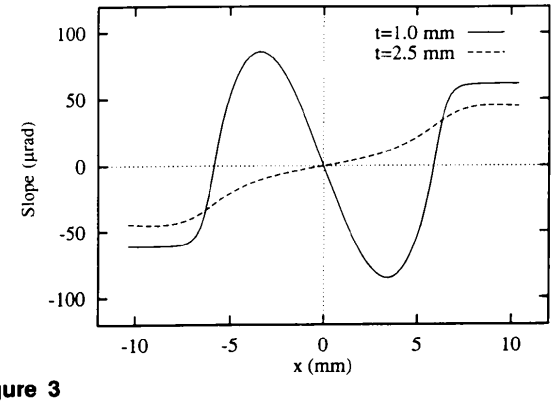


**Figure 3**
Quantitative map showing deformation gradients (surface slope) across the top surface of the silicon crystal having the dimensions described in the text with top lamella thicknesses of $t = 1$ and 2.5 mm.

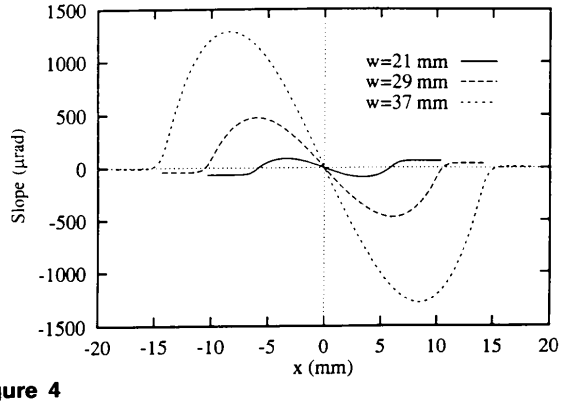


**Figure 4**
Quantitative map showing deformation gradients (surface slope) across the top surface of the silicon crystal having dimensions described in the text with lamella thickness $t = 1$ mm and widths ($w$) shown.

is negative. In all cases, the two outermost regions of the surface simply remain flat but tilt in opposite directions thereby applying the necessary couple to the central lamella. Note that the scales of the deformations are very different in the two cases which derives from the fact that the bending stiffness of the central lamella depends on the cube of its thickness, amounting to a factor of 15.6 for the cases shown.

## 4. Finite-element-analysis model confirmation with laboratory X-rays

In exploratory experiments, we set up a double-crystal diffractometer with two pinhole collimated beams 6 mm apart using the silicon 333 Bragg reflection of Cu $K\alpha$ radiation. The first (sample) crystal was 1.5 mm thick and internally pressurized using air to be positive or evacuated to be negative with respect to atmospheric pressure. The second reference crystal was a perfect thick wafer of float-zone silicon set in the (+–) non-dispersive arrangement with respect to the silicon box sample. Double-crystal two-beam rocking curves obtained with no applied pressure in the sample monochromator box show a single symmetric peak. When the first crystal is pressurized, two peaks are observed separated by an angle $\delta\theta$. The radius of curvature $R$ of the sample, assumed cylindrical, is given by:

$$R = 2X/(\sin\theta_B)\delta\theta = 8.14 \times 10^{-3}/\delta\theta \quad \text{m} \qquad (1)$$

where $2X$ = 6 mm is the pinhole separation and $\theta_B$ is the Bragg angle.

Peak separations *versus* internal hydrostatic pressure are shown halfway to the edge. As expected, the peak separation varies linearly with pressure and the crystal surface is concave when the internal pressure is positive. On the centerline, $y$ = 0, the change of peak separation is approximately 40 arcsec for a pressure change of 132 kPa. These early measurements showed a number of features which led us to develop finite-element-analysis models and more informative laboratory and synchrotron radiation measurement techniques.

The measurements show larger curvatures at the center of the crystal ($y$ = 0) than at $y$ = 20 mm. This crystal, which was tested on the CHESS F2 wiggler beamline (Quintana, Hart *et al.*, 1995) was only 65 mm wide so that the influence of the end wall is substantial at $y$ = 20 mm but vanishes by symmetry on the centerline. As a consequence, later crystals were made 80 mm wide as in Fig. 1. The design is infinitely extensible and is only limited by material availability. Mounting strains are revealed by the peak separation at zero pressure. These are 14 μrad on the centerline and essentially zero parasitic strain at $y$ = 20 mm. Provided that the mounting strain is independent of position on the crystal, it can be cancelled by the appropriate change of water pressure.

These laboratory-based experiments can quantitatively map the entire two-dimensional pressure and mounting strain fields and show, for example, that the mean radius of curvature on the centerline is 51 m at 181 kPa. This follows from Fig. 6 using (1). However, as the finite-element-analysis models show, the surface shape is not necessarily cylindrical so that more detailed methods than simple two-beam double-crystal rocking curves are required.

A more versatile single-beam double-crystal diffractometer in which the X-ray beam can be raster scanned $(x,y)$ across the crystal surface (Quintana, Dolin, Georgopoulos, & Kushnir, 1995) has been developed. A 2.0 mm thick crystal has been tested under the high heat load from an undulator on the DORIS bypass at HASYLAB (Quintana, Hart *et al.*, 1995). We have made raster-scanned measurements of the Bragg angle along the midline of that crystal (Fig. 7). Except for the region above the walls of the box, the surface of the crystal exhibits a concave shape. In modeling the deformations using the same assumptions that were performed in Fig. 2, we found that the measured slope was approximately three times that of the modeled slope. However, if we relax the boundary condition to let the side of the box slide along the stainless-steel

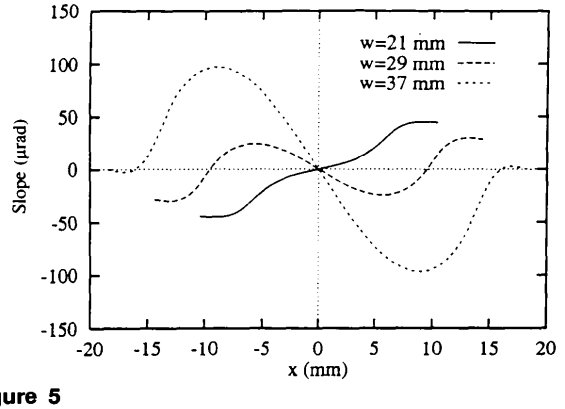


**Figure 5**
Quantitative map showing deformation gradients (surface slope) across the top surface of the silicon crystal having dimensions described in the text with lamella thickness $t$ = 2.5 mm and widths ($w$) shown.

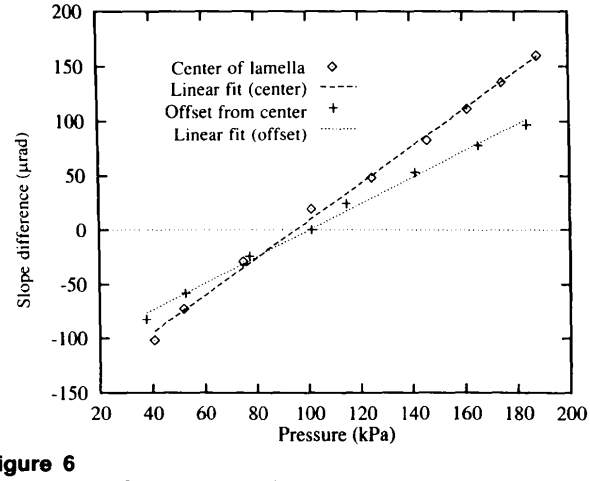


**Figure 6**
The position of two-beam double-crystal rocking curves at various internal pressures for a 1.5 mm thick lamella silicon-crystal box. Pressure is the absolute hydrostatic pressure inside the box with 101 kPa pressure outside the box.

base by 1 μm, then we reproduce the overall slope as well as the expected sigmoidal shape similar to that seen in the $t$ = 2.5 mm plot of Fig. 3. The assumed amount of sliding is approximately 20% of the value the box would have if it were totally unconstrained along the surface of the base. We can expect a certain amount of sliding since the silicone rubber is more compliant than the silicon. In fact, the crystal performs better than expected since the sliding introduces an additional slope on the lamella which causes it to bend into a concave shape. However, the excellent agreement between the actual and modeled response demonstrates our understanding of the important variables in this monochromator design which is essential in designing monochromator systems which have exacting tolerances (*i.e.* a few to tens of microradians) and through which future designs can benefit. Future designs will incorporate a monolithic silicon girdle around the base of the matchbox as part of an indium water seal; this will also better control this boundary condition.

## 5. Conclusions and improvements

The combination of finite-element techniques with double-crystal rocking-curve measurements on real crystals offers an extremely powerful tool in determining the important variables in the design of adaptive optics systems. This is especially important when trying to achieve the tolerances of some tens of microradians over ranges of up to hundreds of microradians required in double-crystal monochromators. The combination of these techniques has resulted in significant progress in determining the important variables in crystal optics design. While extensions to the overall adaptive box design using actuators have recently been proposed (Schulte-Schrepping, Materlik, Heuer, & Teichmann, 1995), we have optimized an adaptive design for high-power wiggler sources which contain no in-vacuum motions or transducers which may degrade from radiation damage. Even though silicone rubber has been used successfully in several monochromators at the Daresbury SRS (Cernik & Hart, 1989), it is not compatible with ultra-high vacuum designs and, as is shown, can affect the mechanical boundary conditions of the modeling. Consequently, even though mounting the crystal with silicone rubber improves the overall box design, a better choice would be a strain-free 'hard' seal which will allow us to more accurately control the mechanical boundary conditions and is the next logical step in design improvement. Other variables to be optimized are the lamella thickness profile to compensate for distortions beyond second order (*i.e.* cylindrical) in conjunction with frustrated edge cooling to cause the top surface of the lamella to be more isothermal.

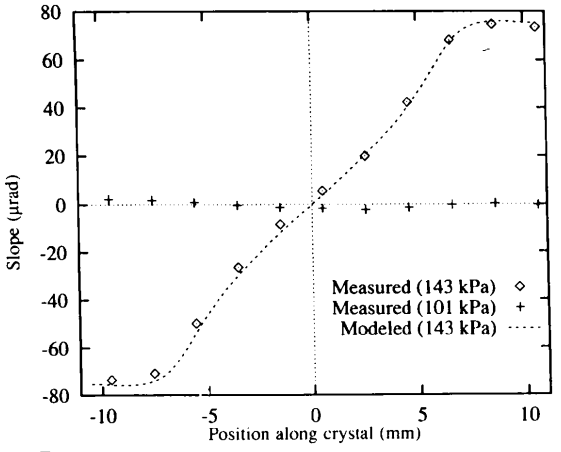


**Figure 7**
Raster-scanned double-crystal Bragg-angle map on a 2.0 mm thick lamella silicon box with absolute internal pressures of 101 and 143 kPa along with finite-element modeling results assuming that the base is allowed to slide by 1 μm. The pressure external to the box is 101 kPa.

This work was supported in part by the National Science Foundation through Grant INT-9008189 and through the DND-CAT Synchrotron Research Center at Northwestern University which, in turn, is supported by the E. I. Du Pont de Nemours and Co., The Dow Chemical Co., the State of Illinois through the Higher Education Cooperation Act Grant, and the National Science Foundation through Grant DMR-9304725.

## References

Berman, L. E. & Hart, M. (1991*a*). *Nucl. Instrum. Methods*, **A300**, 415–421.
Berman, L. E. & Hart, M. (1991*b*). *Nucl. Instrum. Methods*, **A302**, 558–562.
Berman, L. E. & Hart, M. (1993). *Nucl. Instrum. Methods*, **A334**, 617–620.
Berman, L. E., Hart, M. & Sharma, S. (1992). *Nucl. Instrum. Methods*, **A321**, 617–628.
Berman, L. E. & Hastings, J. B. (1992). *SPIE J.* **1739**, 489–501.
Berman, L. E., Hastings, J. B., Siddons, D. P., Koike, M., Stojanoff, V. & Hart, M. (1993). *Nucl. Instrum. Methods*, **A329**, 555–563.
Bilderback, D. H. (1986). *Nucl. Instrum. Methods*, **A246**, 434–436.
Cernik, R. & Hart, M. (1989). *Nucl. Instrum. Methods*, **A281**, 403–405.
Chrzas, J., Khounsary, A. M., Mills, D. M. & Vicarro, P. J.(1990). *Nucl. Instrum. Methods*, **A291**, 300–304.
Hart, M. (1990). *Nucl. Instrum. Methods*, **A297**, 306–311.
Marot, G., Rossat, M., Freund, A., Joksch, S., Kawata, H., Chang, L., Ziegler, E., Berman, L., Chapman, D. & Larocci, M. (1992). *Rev. Sci. Instrum.* **63**, 477–480.
Quintana, J. P., Dolin, Yu., Georgopoulos, P. & Kushnir, V. I. (1995). *Rev. Sci. Instrum.* **66**, 2188–2189.
Quintana, J. P., Hart, M., Bilderback, D., Henderson, C., Richter, D., Setterson, T., White, J., Hausermann, D., Krumrey, M. & Schulte-Schrepping, H. (1995). *J. Synchotron Rad.* **2**, 1–5.
Schulte-Schrepping, H., Materlik, G., Heuer, J. & Teichmann, T. (1995). *Rev. Sci. Instrum.* **66**, 2217–2219.
Sharma, S., Berman, L. E., Hastings, J. B. & Hart, M. (1992). *SPIE J.* **1739**, 604–614.
Smithers, R. K. (1989). *Rev. Sci. Instrum.* **60**, 2044–2047.
Swanson Analysis Systems Inc. (1994). *ANSYS*. Swanson Analysis Systems Inc., Houston, Pennsylvania, USA.
Wortman, J. J. & Evans, R. A. (1965). *J. Appl. Phys.* **36**(1), 153–156.
Zhang, L. (1993). *SPIE J.* **1997**, 223–235.